



Electrospinning-derived carbon fibrous mats improving the performance of commercial Pt/C for methanol oxidation

Miaoyu Li, Shizhen Zhao, Gaoyi Han*, Binsheng Yang*

Institute of Molecular Science, Key Laboratory of Chemical Biology and Molecular Engineering of Education Ministry, Shanxi University, Taiyuan 030006, PR China

ARTICLE INFO

Article history:

Received 25 November 2008
Received in revised form 23 January 2009
Accepted 28 January 2009
Available online 7 February 2009

Keywords:

Electrospinning
Carbon nanofibers
Methanol
Electro-oxidation
Impedance

ABSTRACT

The carbon fibrous mats (CFMs) formed by carbon nanofibers whose average diameter is about 150 nm have been fabricated by thermally treating the electrospun polyacrylonitrile fibrous mats. The electrocatalytic activity of commercial Pt/C supported on the CFMs for methanol oxidation in a sulfuric acid solution has been investigated by cyclic voltammetry, chronoamperometry, quasi-steady state polarization, and electrochemical impedance spectroscopy (EIS) methods. The results show that the commercial Pt/C supported on the CFMs exhibits higher electrocatalytic activity, more stability, larger exchange current and smaller charge transfer resistance than that on commercial carbon papers (CPs), which reveals that the CFMs could be developed as suitably-supporting materials for Pt/C catalyst due to their special porous and continuous fibrous structures.

© 2009 Elsevier B.V. All rights reserved.

1. Introduction

In recent years, direct methanol fuel cells (DMFCs) have been considered as one of the most promising power sources due to their potential applications in transportation and portable electronic devices [1–4]. At present, platinum and its alloy are usually used as the cathode and anode catalysts for the oxygen reduction and methanol oxidation in DMFCs, respectively. However, the industrialization of DMFCs is still restricted by two key problems: the high cost of catalysts and the low methanol electrocatalytic oxidation kinetics caused by the catalyst poisoning. Thus, it is necessary to improve the catalytic activity of platinum for methanol electro-oxidation and minimize its use simultaneously [5]. To solve these problems, various carbon materials such as mesoporous carbon, carbon nanotubes, carbon nanofibers, and mesocarbon microbeads have been used as the supports for platinum catalysts of DMFCs [6,7]. But up to now, it still remains challenging to develop alternate electrode materials for better activity and stability for methanol electro-oxidation.

It is well known that fibrous catalytic packs can usually display such advantages as immobile catalyst, short diffusion distance and the low resistance for liquid and gases flow through the bundle of fibers, so they would be used as an attractive alternative material in DMFCs [6]. Recently, electrospinning technique has been recognized as an efficient method to produce the webs of

nanofibers for application in electrodes, sensing and tissue engineer [8–13]. By using a judicious combination of electrospinning and thermal treatment, conducting carbon webs can be conveniently fabricated and used as an ideal candidate for the electrode material of high-power lithium-ion batteries (LIBs) and supercapacitor [8–11]. The special structure and the reported applications for the carbon nanofibrous materials considered, it will be interesting to use the carbon fibrous mats (CFMs) directly as commercial Pt/C catalyst supports in the DMFCs field. So in this paper, the CFMs loaded with commercial Pt/C (Pt/C-CFMs) are used as catalytic electrodes and their performances for methanol electro-oxidation have been evaluated detailedly. Reason for the higher performance of the Pt/C-CFMs catalytic electrodes has also been illuminated.

2. Experimental

2.1. Reagents

Polyacrylonitrile (PAN) and Nafion solution (5%) were obtained from Aldrich. The commercial Pt/C (40 wt.%) was obtained from Johnson Matthey Corp. and the commercial carbon paper (CP) (HCP-020P, 190 μm) was obtained from Ballard Material Products Corp. All other chemicals employed in this study were of analytical grade.

2.2. Apparatus

Scanning electron microscopy (SEM) micrographs were taken on JEOL-JSM-6700F scanning electron microanalyser at 15 kV

* Corresponding authors. Tel.: +86 351 7016358; fax: +86 351 7016358.
E-mail address: han.gaoyis@sxu.edu.cn (G. Han).

accelerated volt. XRD patterns were recorded on Bruker D8 Advance X-ray diffractometer (Cu K α radiation) at 0.02° S⁻¹ scan rate. The electrical conductivity was measured by using the four-point probe method. The specific surface area and pore parameters were determined on a mercury injection apparatus (PASCAL 140/240, CE), the used pressure ranged from atmospheric pressure to 200 MPa at 25 °C. The mechanical properties of the CFMs and commercial CP have been evaluated with an electronic mechanical omnipotent test-bed (SANS CMT7104) and all the tests were performed at a strain ramp rate of 1.0 mm min⁻¹. Electrochemical measurements were carried out on a CHI 660B electrochemistry workstation at 25 °C. Electrochemical impedance spectroscopy (EIS) was performed with amplitude of 5 mV in the frequency range 100 KHz to 0.1 Hz and was carried out at different potentials. The Zview-2 fitting program was used to analyze the impedance parameters. The CFMs or the commercial carbon paper loaded with commercial Pt/C catalyst, a platinum plate and a saturated calomel electrode (SCE) were used as working, counter and reference electrode, respectively. High-purity argon flow was used for deaerating the solutions and maintained above the electrolyte solution during measurements.

2.3. Fabrication of CFMs and electrodes

The CFMs were fabricated according to the previously reported method [14] except that the thickness of the CFMs was about 190 μm in this paper. The resulted CFMs were cut into strips with the size of 10 mm \times 2.0 mm and used as electrodes directly. Pt/C-CFMs electrodes were fabricated by transferring 6.4 μl of the ultrasonic-treated mixture of Pt/C catalyst (5.0 mg), water (1.25 ml) and Nafion solution (5%, 0.25 ml) onto the CFMs, and then evaporating the solvent at the room temperature. By comparison, the same amount of commercial Pt/C was loaded on the commercial CP and these electrodes were labeled as Pt/C-CP electrodes. The content of Pt loaded on the Pt/C-CFMs and Pt/C-CP electrodes was

about 0.21 mg cm⁻². And the geometric surface area of the catalytic electrodes was guaranteed to be about 0.04 cm².

3. Results and discussion

3.1. Characterization of the Pt/C-CFMs and Pt/C-CP electrodes

The typical morphology of the obtained CFMs is shown in Fig. 1A. From the scanning electron microscopy (SEM) images, we can find clearly that the CFMs are formed by long fibers with smooth surface whose diameter may range from 130 to 170 nm (average 150 nm). There are a large number of gaps in the mats, which is beneficial to disperse catalysts and diffuse reactant. Fig. 1B shows the SEM image of Pt/C-CFMs electrodes, from which we find that the surface of CFMs is coated with Pt/C catalyst particles uniformly and the gaps dispersed in the mat have disappeared. From the SEM images of the commercial CP (Fig. 1C), we find that the diameter of the carbon fibers is about 8 μm which is far bigger than that of CFMs, and that many large gaps are observed in the commercial CP, moreover, some gaps are filled by the bond that causes the carbon fibers to conglutinate together. From the SEM images of the Pt/C-CP (Fig. 1D), we can find that the Pt/C catalyst particles form a very coarse coating on the CP surface and some large cracks are observed further. From Fig. 1B and D, we can conclude that Pt/C catalysts disperse more evenly on the surface of CFMs than on the surface of commercial CP. From the typical XRD patterns of samples displayed in Fig. 2, it is clear that the as-prepared CFMs exhibit a broad XRD diffraction peak at about 25.3° corresponding to the (002) plane diffraction of graphite crystallite [6]. However, the commercial CP shows a strong and narrow XRD diffraction peak at about 26.5°, which indicates that the commercial CP is a higher graphitized carbon than CFMs. After the CFMs and commercial CP are coated with commercial Pt/C catalyst, the electric conductivities of Pt/C-CFMs and Pt/C-CP electrodes are measured and found to be \sim 52 S cm⁻¹ and 86 S cm⁻¹, which are 5.4% and 11.3% smaller than those of CFMs

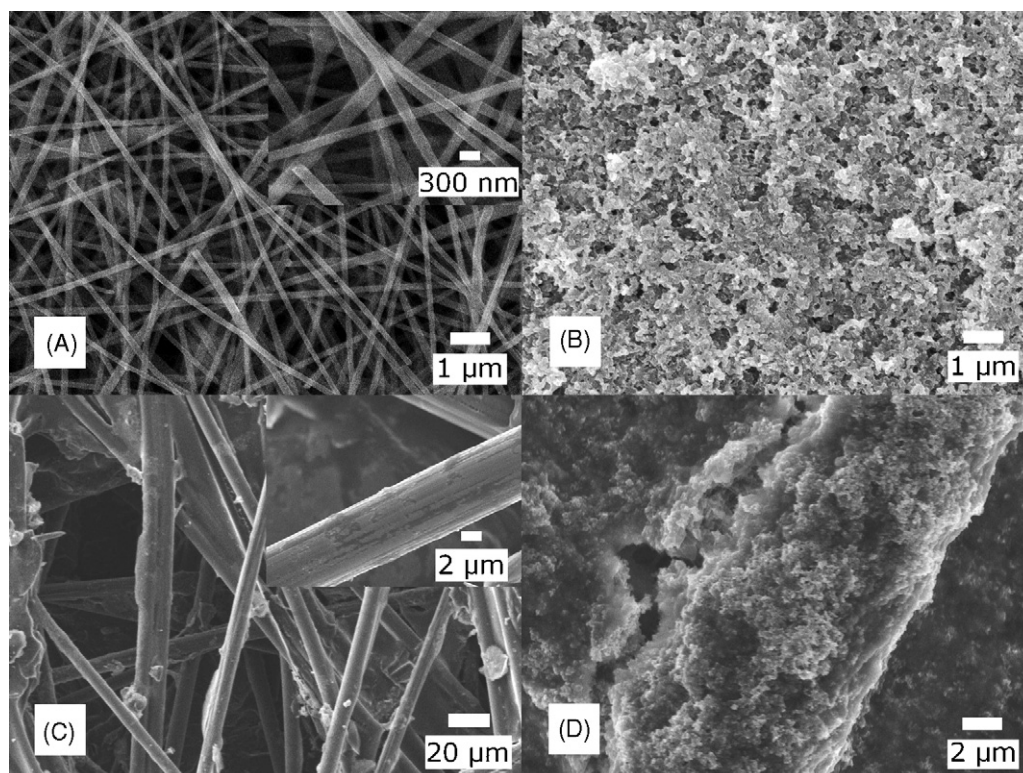


Fig. 1. The SEM images of (A) CFMs, (B) Pt/C-CFMs electrode, (C) CP and (D) Pt/C-CP electrode.

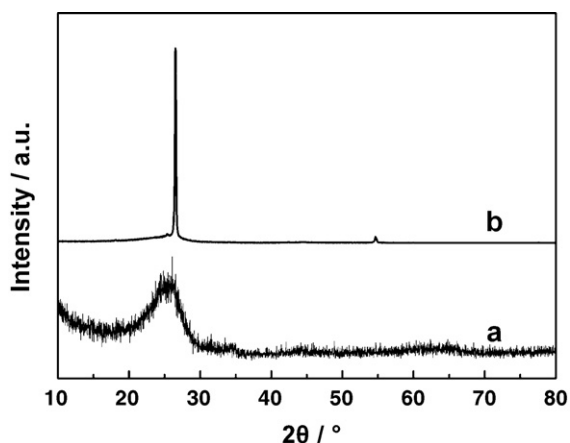


Fig. 2. The XRD patterns of the (a) as prepared CFMs and (b) the commercial CP.

(55 S cm^{-1}) and CP (97 S cm^{-1}). The thicknesses of Pt/C-CFMs and Pt/C-CP electrodes are also measured and found to be about 197 and $205 \mu\text{m}$, which are about 7 and $15 \mu\text{m}$ thicker than CFMs and CP, respectively. The above mentioned results reveal that the commercial Pt/C catalyst exhibits lower conductivities than CFMs and CP, which causes a decrease in the conductivity of the Pt/C-CFMs and Pt/C-CP electrode; and that more commercial Pt/C catalyst are filled in the gaps of the CFMs, which causes a little increase in the thickness of the Pt/C-CFMs in comparison with the Pt/C-CP electrode.

In order to clarify the phenomena above mentioned and evaluate the practicability of the CFMs, the physical properties of CFMs and CP are measured at the same time. Fig. 3 shows the pore size distributions for CFMs and commercial CP at 25°C , from which we can find that the commercial CP contains mainly the large pores whose sizes are larger than $2 \mu\text{m}$, while the CFMs contain not only the large pores whose sizes are larger than $2 \mu\text{m}$ (55%) but also the small pores whose sizes are smaller than $2 \mu\text{m}$ (45%). The results also show that the specific surface area, total pore volume and porosity of the CFMs are $22.84 \text{ m}^2 \text{ g}^{-1}$, 2.94 ml g^{-1} and 65%, respectively, which are larger than the specific surface area ($4.64 \text{ m}^2 \text{ g}^{-1}$), total pore volume (0.24 ml g^{-1}) and porosity (29%) of the commercial CP because the CFMs are formed by nanofibers. So the Pt/C particles disperse in the CFMs more easily than in commercial CP. The tensile, compressive and rupture strengths of CFMs are about 12.09, 16.02 and 38.67 MPa , respectively, which are slightly larger than the tensile, compressive and rupture strength of CP: 11.49, 15.56 and 35.85 MPa . The mechanical strength data indicate that the CFMs exhibit enough mechanical strength to endure the pressure to make the MEA electrodes.

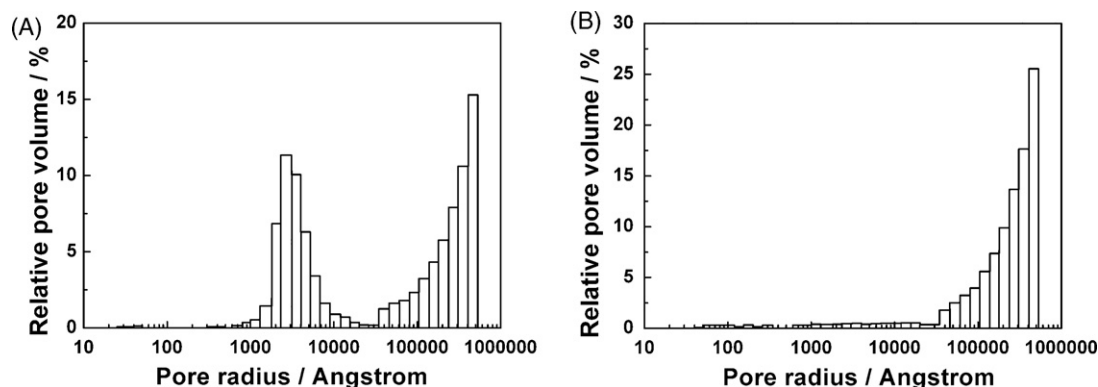
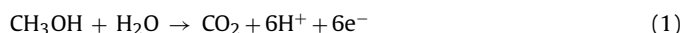


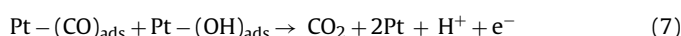
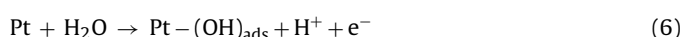
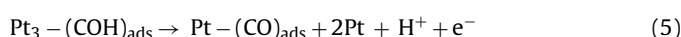
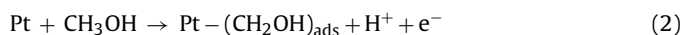
Fig. 3. Pore size distributions for (A) CFMs and (B) commercial CP at 25°C .

3.2. Electrochemical properties of Pt/C-CFMs and Pt/C-CP electrodes

In $0.5 \text{ mol L}^{-1} \text{ H}_2\text{SO}_4$ and $1.0 \text{ mol L}^{-1} \text{ CH}_3\text{OH}$ aqueous solutions, the curves for CFMs and CP electrodes show no significant redox activity ((a) and (b) in Fig. 4A). However, the anodic current density on Pt/C-CFMs electrode ((d) in Fig. 4A) in the positively going scan increases with the increase of scan potential, and the peak current density reaches about 90.20 mA cm^{-2} at 0.67 V which is significantly higher than 65.13 mA cm^{-2} at 0.66 V on Pt/C-CP electrode ((c) in Fig. 4A). In the reverse scan there is an anodic peak observed on both Pt/C-CFM and Pt/C-CP electrodes, which can be attributed to the removal of the incompletely oxidized carbonaceous species formed in the positively going scan [7]. The electro-oxidation of methanol has been studied extensively and the anodic oxidation of methanol can be written [15–17] as:



In acid media the reaction has been suggested to proceed according to the following series of steps:



The anodic peak current densities in the positively going and negatively going scan are defined as I_f and I_b and the value of I_f/I_b can be used to evaluate the tolerance of catalyst to the accumulation of the carbonaceous species. There is no obvious difference between the Pt/C-CFMs electrode (0.79) and the Pt/C-CP electrode (0.80) because the same catalysts are used in these two kinds of electrocatalytic electrodes [18,19].

Fig. 4B shows the anodic peak current densities of methanol oxidation on Pt/C-CFMs and Pt/C-CP electrodes during a total of 700 cycles in $0.5 \text{ mol L}^{-1} \text{ H}_2\text{SO}_4$ and $1.0 \text{ mol L}^{-1} \text{ CH}_3\text{OH}$ solutions. For both the electrodes, the anodic peak current density in positively going scan increases at initial cycles until it attains the maximum value and afterwards displays a downward trend with the successive CV scans. For Pt/C-CFMs electrode, the peak current density approaches a maximum (about 98.46 mA cm^{-2}) at the 41st cycle, and then decreases to about 50.21 mA cm^{-2} at the 700th cycle, with a total decrease of 49.00%. However, the peak current density reaches its maximum (about 68.32 mA cm^{-2}) at the 66th cycle for Pt/C-CP electrode, and then decreases to 32.16 mA cm^{-2}

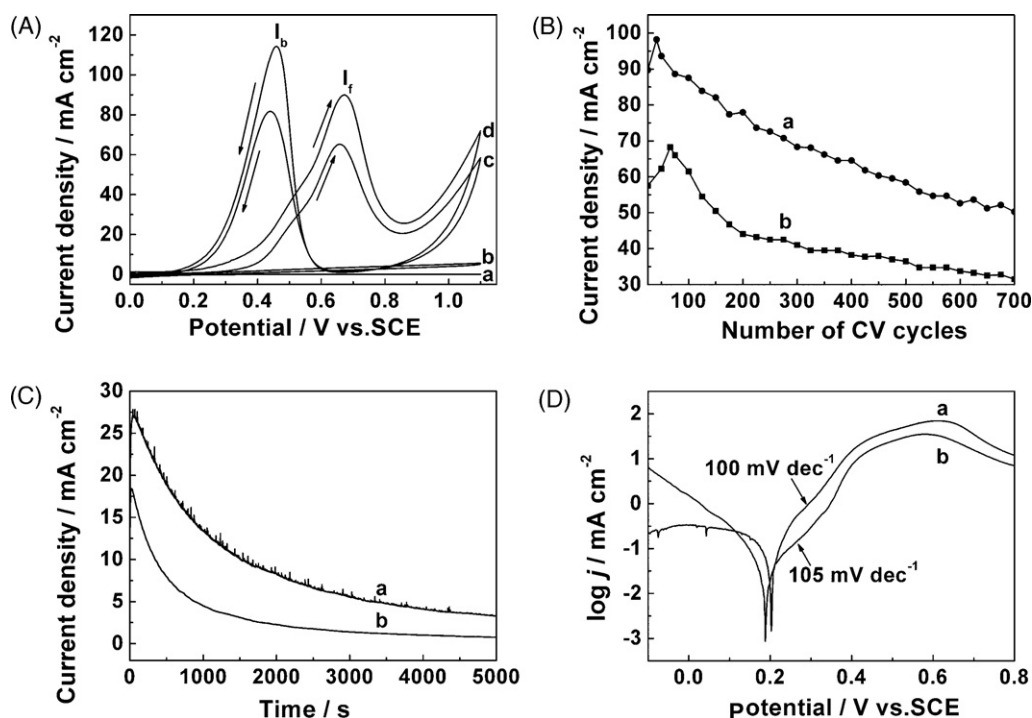


Fig. 4. (A) Cyclic voltammograms obtained for methanol oxidation on (a) CFMs, (b) CP, (c) Pt/C-CP, (d) Pt/C-CFMs electrodes with the potential scan rate of 50 mV s^{-1} , (B) the plot of anodic peak current density of methanol oxidation on (a) Pt/C-CFMs and (b) Pt/C-CP electrodes versus cycle numbers of CV with the potential scan rate of 100 mV s^{-1} , (C) chronoamperometric curves of methanol oxidation on (a) Pt/C-CFMs and (b) Pt/C-CP at potential of 0.45 V (versus SCE), (D) Tafel plots for methanol oxidation on the (a) Pt/C-CFMs and (b) Pt/C-CP at a potential scan rate of 2 mV s^{-1} . The electrolyte is $0.5 \text{ mol L}^{-1} \text{ H}_2\text{SO}_4 + 1.0 \text{ mol L}^{-1} \text{ CH}_3\text{OH}$ aqueous solution.

at the 700th cycle, with a total decrease of 52.92%. The peak current density loss may result from the consumption of the CH_3OH in solution during the CV scans and be also due to the poisoning and structure changing of Pt catalysts which usually leads to a decrease of the catalytic activity. The above results indicate that the Pt/C-CFMs electrode exhibits better long-term stability than Pt/C-CP electrode. Fig. 4C shows the curves of polarization current density of methanol oxidation versus time at a constant potential 0.45 V in $0.5 \text{ mol L}^{-1} \text{ H}_2\text{SO}_4$ and $1.0 \text{ mol L}^{-1} \text{ CH}_3\text{OH}$ solutions. After the current densities reach their maximums, the current densities of methanol oxidation on both Pt/C-CFMs and Pt/C-CP electrodes present continuous decay as time goes on. After a polarization time of 1000 s , the current densities are 13.41 and 4.53 mA cm^{-2} for Pt/C-CFMs and Pt/C-CP electrodes, respectively. In addition, the decay of the current density on Pt/C-CFMs electrode exhibits a more gently decreasing trend. After a polarization time of 5000 s , there are 8.30 and 2.32 mA cm^{-2} current densities remained on Pt/C-CFMs and Pt/C-CP electrodes, respectively. It is clear that the remained current density on the Pt/C-CFMs electrode is higher than that on the Pt/C-CP electrode, which is in accordance with the results shown in Fig. 4A and B, denoting a strong electrocatalytic behavior towards methanol oxidation on Pt/C-CFMs electrode. The reason may be that the CFMs contain larger specific surface area ($22.84 \text{ m}^2 \text{ g}^{-1}$) and larger pore volume (2.94 ml g^{-1}) than commercial CP (specific surface area $4.64 \text{ m}^2 \text{ g}^{-1}$ and pore volume 0.24 ml g^{-1}), which will be advantageous to a better dispersion of catalysts. Furthermore, in comparison with the commercial CP, the CFMs contain not only the large pores but also the small pores, which will increase the three-dimensional interaction between the catalyst and the fibers of CFMs. The two points mentioned above enable the catalyst to be dispersed well and keep a good contact between the nanofibers and the catalyst particles during the process of experiment, which make the Pt/C-CFMs exhibit better long-term stability.

In order to investigate catalytic activities of Pt/C-CFMs electrode and Pt/C-CP electrode, the exchange current densities (j_0)

for methanol oxidation are calculated. The polarization studies for Pt/C-CFMs and Pt/C-CP electrodes have been carried out in $0.5 \text{ mol L}^{-1} \text{ H}_2\text{SO}_4$ and $1.0 \text{ mol L}^{-1} \text{ CH}_3\text{OH}$ solutions, and the Tafel curves are shown in Fig. 4D. According to the Tafel equation [13]:

$$\eta = a + b \log j$$

$$a = -\frac{2.303RT}{\beta nF} \log j_0, \quad b = \frac{2.303RT}{\beta nF} \quad (8)$$

Where $\eta = E - E_{\text{eq}}$ is named as the overpotential and β is the anodic charge transfer coefficient. Then j_0 can be calculated by using $j_0 = 10^{-a/b}$ according to the relationship between η and $\log j$. The values of j_0 are calculated with the same procedure to be 123.07 and $27.43 \mu\text{A cm}^{-2}$ for Pt/C-CFMs and Pt/C-CP electrode, respectively. The j_0 value on Pt/C-CFMs electrode is about 4.49 times as large as that on Pt/C-CP electrode. And the slopes of the Tafel curve are approximately 100 and 105 mV dec^{-1} for methanol oxidation on Pt/C-CFMs and Pt/C-CP electrode, respectively.

In order to obtain more information about methanol oxidation reaction on Pt/C-CFMs and Pt/C-CP electrodes, the relationships between anodic peak current density (I_p) and peak potential (E_p) obtained from forward CV scans with different sweep rates (ν) have also been studied and the plots are shown in Fig. 5. It is clear that there is a linear relationship between I_p and $\nu^{1/2}$ for Pt/C-CFMs and Pt/C-CP electrodes (Fig. 5A). This may imply that the process of methanol oxidation is controlled by diffusion process of methanol [7,20]. Additionally, it can also be observed that the slope of lines at smaller scan rates (I_a and I_b) is larger than that at larger scan rates (II_a and II_b) for the both electrodes. However, the slope of line I_a for Pt/C-CFMs electrode is 24.5 , which is six times as large as that of line I_b (4.1) for Pt/C-CP electrode. And the slope of line II_a for Pt/C-CFMs electrode is 1.60 , which is also twice the size of line II_b (0.86) for Pt/C-CP electrode. Fig. 5B shows the dependent relation of peak potential (E_p) for methanol oxidation upon the $\ln(\nu)$ at the electrodes. In Fig. 5B, E_p of the methanol oxidation

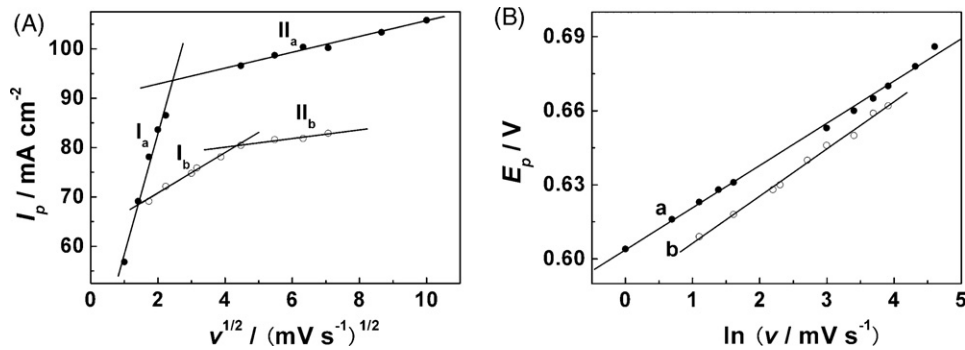


Fig. 5. (A) The plots of peak current density versus square root of sweep rates (lines I_a and II_a for Pt/C-CFMs electrode; lines I_b and II_b for Pt/C-CP electrode) and (B) E_p versus $\ln(v)$ at different electrodes of (a) Pt/C-CFMs and (b) Pt/C-CP in $0.5 \text{ mol L}^{-1} \text{ H}_2\text{SO}_4 + 2.0 \text{ mol L}^{-1} \text{ CH}_3\text{OH}$.

at both Pt/C-CFMs and Pt/C-CP electrodes are shifted positively when v increases. And the linear relationship between E_p and $\ln(v)$ can be observed obviously, which indicates that the oxidation of methanol is an irreversible electrode process. The linear slope for Pt/C-CFMs electrode (0.017) is smaller than that for Pt/C-CP electrode (0.019). From the above results, we can also deduce that Pt/C-CFMs electrode has stronger electrocatalytic behavior towards methanol oxidation than Pt/C-CP electrode.

EIS is the ac impedance as a function of the ac sources frequency, from which the charge transfer resistance (R_{ct}) will be obtained [21], so EIS measurements are carried out to evaluate charge transfer property of methanol oxidation over the Pt/C-CFMs and Pt/C-CP electrodes. From the complex plots of the impedance shown in Fig. 6, we find that all the complex plots of the impedance consist of two semicircles or arcs in which the small ones at the high frequency are independent of potentials and may be associated with a double charging effect, whereas the large ones at low frequency appear to vary with potentials and may associate with the R_{ct} which is related to the charge transfer reaction kinetics. Furthermore, we can also find that the semicircles in low frequency range for Pt/C-CFMs electrode show smaller diameter than

that for Pt/C-CP electrode. The impedance plots at 0.32 V show capacitive behaviors and signify a reaction with one adsorbed intermediate (Fig. 6A). The impedance data can be simulated through the equivalent circuit shown in Fig. 6D(a). So the assumption that methanol dehydrogenation is rate-determining step should be reasonable [21,22]. On the other hand, the Tafel slopes of the methanol electro-oxidation from Fig. 4D are close to 118 mV dec^{-1} at 0.32 V for both the two electrodes, indicating that the rate-determining step is the first electron process. At about 0.40 V, impedance data plotted in the complex plane extend into the fourth quadrant, the Nyquist plots are featured by an inductive loop in low frequency range for both electrodes because of the inductive behavior (Fig. 6B), at this potential, the oxidation and removal of CO_{ads} become rate-determining step [22]. The equivalent circuit shown in Fig. 6D(b) can be used to simulate the impedance data. The R_{ct} obtained from simulation of the impedance spectra is 17.62 and $34.42 \text{ } \Omega \text{ cm}^2$ for Pt/C-CFMs and Pt/C-CP electrodes, therefore it is proved that much faster charge transfer rates occur during methanol electro-oxidation on Pt/C-CFMs electrode. When the potential increases to 0.46 V, the main semicircle at low frequency in Nyquist plot flips over to the second quadrant

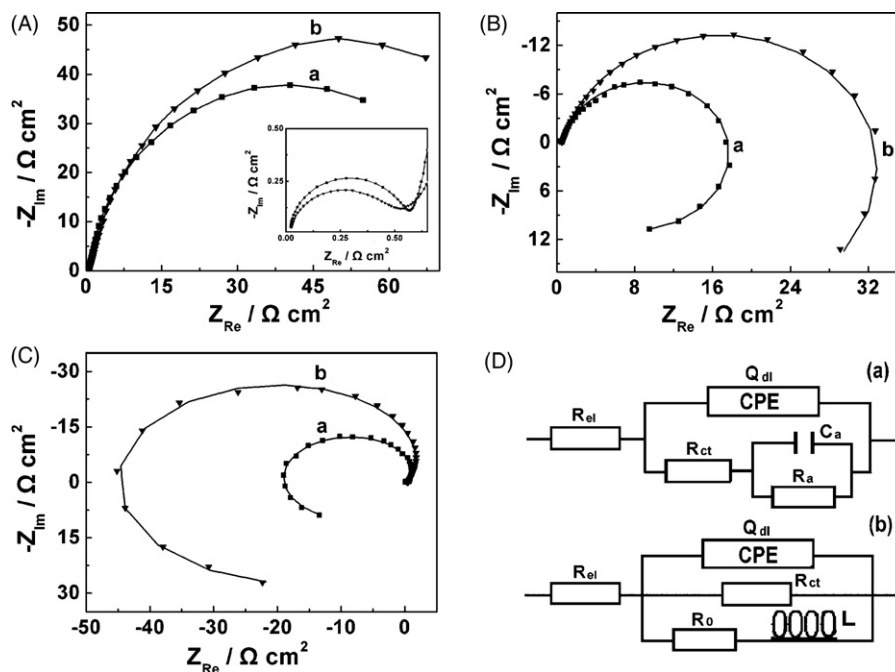


Fig. 6. Complex plane plots of the impedance of the (a) Pt/C-CFMs and (b) Pt/C-CP electrodes in $0.5 \text{ mol L}^{-1} \text{ H}_2\text{SO}_4 + 1.0 \text{ mol L}^{-1} \text{ CH}_3\text{OH}$ at potential (A) 0.32 V, (B) 0.40 V and (C) 0.46 V versus SCE, respectively. The lines represent the fit of the data to the equivalent circuit shown in (D) for the electro-oxidation of methanol. (A) and (C) fit to the (D)-a and (B) to (D)-b.

and part of real component of the impedance becomes negative (Fig. 6C). The EIS data can also be simulated using the equivalent circuit shown in Fig. 6D(a). This means that resistance R_{ct} becomes negative, which results from passivation of electrode surface [22,23].

According to the above mentioned experiments, we can conclude that the high performance of the Pt/C-CFMs electrode mainly comes from the special structures of the CFMs. The commercial Pt/C catalyst particles can easily disperse in the large ($>2 \mu\text{m}$) and small ($<2 \mu\text{m}$) gaps of the mats, which will cause the catalyst particles to contact closely to the fibers and make the electrode more compact, so the charge transfer resistance for methanol oxidation decreases obviously on Pt/C-CFMs electrode.

4. Conclusions

The CFMs loaded with commercial Pt/C catalyst have been used as electrocatalytic electrode for methanol oxidation, and the results show that Pt/C catalyst supported on CFMs exhibits high performance in the aspects of electrocatalytic activity and stability towards the oxidation of methanol. Additionally, the kinetic studies about methanol oxidation on the electrodes show that the Pt/C-CFMs electrodes exhibit higher exchange current and smaller charge transfer resistance than Pt/C-CP electrodes. This may be attributed to the particular properties of carbon nanofibers webs such as the continuity of carbon nanofibers and the unique nanosized porous structure. The nanosized gaps are favorable to make the Pt/C catalyst particles dispersed into the fibrous mats and make the catalyst particles contact closely with the continuous carbon nanofibers and lead to a small contact resistance between the catalyst particles and the supporting materials, which will result in a small charge transfer resistance and large exchange current density. The CFMs could be developed as highly efficient supporting materials for commercial noble metal catalyst used in DMFCs.

Acknowledgments

The authors thank the National Natural Science Foundation of China (no. 20604014) and Shanxi province (no. 2007021008), Foundation for Young Scholar of Shanxi Province (TYAL) and Shanxi University.

References

- [1] H.Q. Song, X.P. Qiu, X.X. Li, F.S. Li, W.T. Zhu, L.Q. Chen, *J. Power Sources* 170 (2007) 50–54.
- [2] J.K. Lee, J. Choi, S.J. Kang, J.M. Lee, Y. Tak, J. Lee, *Electrochim. Acta* 52 (2007) 2272–2276.
- [3] R.Z. Yang, X.P. Qiu, H.R. Zhang, J.Q. Li, W.T. Zhu, Z.X. Wang, X.J. Huang, L.Q. Chen, *Carbon* 43 (2005) 11–16.
- [4] J.Y. Liu, J.Y. Cao, Q.H. Huang, X.W. Li, Z.Q. Zou, H. Yang, *J. Power Sources* 175 (2008) 159–165.
- [5] C. Wang, M. Waje, X. Wang, J.M. Tang, R.C. Haddon, Y.S. Yan, *Nano Lett.* 4 (2004) 345–348.
- [6] H.X. Huang, S.X. Chen, C.E. Yuan, *J. Power Sources* 175 (2008) 166–174.
- [7] M.W. Xu, G.Y. Gao, W.J. Zhou, K.F. Zhang, H.L. Liu, *J. Power Sources* 175 (2008) 217–220.
- [8] C. Kim, K.S. Yang, M. Kojima, K. Yoshida, Y.J. Kim, Y.A. Kim, M. Endo, *Adv. Funct. Mater.* 16 (2006) 2393–2397.
- [9] C. Kim, K.S. Yang, *Appl. Phys. Lett.* 83 (2003) 1216–1218.
- [10] G.Y. Han, B. Guo, L.W. Zhang, B.S. Yang, *Adv. Mater.* 18 (2006) 1709–1712.
- [11] W.X. Zhang, Y.Z. Wang, C.F. Sun, *J. Polym. Res.* 14 (2007) 467–474.
- [12] A. Greiner, J.H. Wendorff, *Angew. Chem. Int. Ed.* 46 (2007) 5670–5703.
- [13] B. Guo, S.Z. Zhao, G.Y. Han, L.W. Zhang, *Electrochim. Acta* 53 (2008) 5174–5179.
- [14] M.Y. Li, G.Y. Han, B.S. Yang, *Electrochem. Commun.* 10 (2008) 880–883.
- [15] J.B. Goodenough, A. Hamnett, B.J. Kennedy, S.A. Weeks, *Electrochim. Acta* 32 (1987) 1233–1238.
- [16] B.J. Kennedy, A. Hamnett, *J. Electroanal. Chem.* 283 (1990) 271–285.
- [17] A.H. Su, C.Z. Li, G.Q. Sun, Y. Zhang, T.H. Lu, *Chin. J. Power Sources* 19 (1995) 31–35.
- [18] G.Y. Zhao, C.L. Xu, D.J. Guo, H. Li, H.L. Li, *J. Power Sources* 162 (2006) 492–496.
- [19] L. Zhang, D. Xia, *Appl. Surf. Sci.* 252 (2006) 2191–2195.
- [20] H. Tang, J.H. Chen, Z.P. Huang, D.Z. Wang, Z.F. Ren, L.H. Nie, Y.F. Kuang, S.Z. Yao, *Carbon* 42 (2004) 191–197.
- [21] E.H. Yu, K. Scott, R.W. Reeve, *J. Electroanal. Chem.* 547 (2003) 17–24.
- [22] G. Wu, L. Li, B.Q. Xu, *Electrochim. Acta* 50 (2004) 1–10.
- [23] V.S. Bagotzky, Y.B. Vassilyev, *Electrochim. Acta* 12 (1967) 1323–1343.